J. Fluid Mech. (2001), *vol.* 430, *pp.* 27–50. Printed in the United Kingdom

© 2001 Cambridge University Press

On the piston and sloshing modes in moonpools

By B. MOLIN

Ecole Supérieure d'Ingénieurs de Marseille, 13451 Marseille cedex 20, France
e-mail: molin@esim.imt-mrs.fr

(Received 28 April 2000 and in revised form 6 September 2000)

So-called 'moonpools' are vertical openings through the deck and hull of ships or barges, used for marine and offshore operations, such as pipe laying or recovery of divers. In the present study rectangular moonpools of large horizontal dimensions are considered. The natural modes of oscillation of the inner free surfaces are determined, under the assumption of infinite water depth and infinite length and beam of the barges that contain the moonpools. The problem is treated in two and three dimensions, via linearized potential flow theory. Results are given for the natural frequencies and the associated shapes of the free surface, for wide ranges of the geometric parameters. Simple quasi-analytical approximations are derived that yield the natural frequencies. The most striking result is that the natural frequencies of the longitudinal sloshing modes increase without bounds when both the draught and the width decrease to zero, the length of the moonpool being kept constant. As a corollary the problem of waves travelling in a channel through a rigid ice sheet is addressed and their dispersion equation is derived. The same behaviour is obtained: the waves travel increasingly faster as both the draught and the width of the channel are reduced.

1. Introduction

The starting point of this analysis is a new barge concept, for offshore oil production in mild seas and large water depths. The oil effluent flows up from the seabed through steel risers, tensioned by buoyancy elements, that terminate within a large central opening in the barge: the 'well-bay'. Typical dimensions of the well-bay, or 'moonpool', are 80 m long and 20 m wide, the barge itself being about three times as long and as wide. The draught can be quite shallow: 5 or 6 m when no storage or processing equipment is required.

A hydrodynamic problem encountered with this concept is the water motion that takes place in the moonpool, under wave-induced pressures and barge motion. This water motion mostly occurs at the natural modes of the moonpool: the *sloshing* modes, back and forth in between the vertical walls (like in a tank), and the *piston* mode, where the water inside the moonpool heaves up and down more or less like a rigid body.

Predictive tools are needed, at the design stage, to calculate the amplitude of these resonant modes, and, beforehand, to precisely locate their frequencies with regard to the frequencies of the most energetic waves. For this state-of-the-art diffraction radiation codes were used and they revealed some hitherto unsuspected features of the resonant frequencies of the longest sloshing modes: their frequencies turned out to be much greater than expected. For instance, with a $80 \times 20 \times 5$ m moonpool, the natural period of the first longitudinal mode is less than 7.5 s, corresponding to a

https://doi.org/10.1017/S0022112000002871 Published online by Cambridge University Press

wavelength of 85 m in an unbounded ocean, nowhere near twice the length of the moonpool!

It is this problem, of calculating the natural frequencies, and associated free surface shapes, that we are concerned with in this paper. It is solved under the simplifying assumption that the length and beam of the barge are much larger than the length and width of the moonpool, so they are taken to be infinite. As a result the fluid domain divides into two subdomains: the moonpool, extending vertically from $z = 0$ to $z = h$, where h is the draught, of length l and width b, and the semi-infinite half space $z \leqslant 0$. The barge is assumed to be motionless.

The problem is tackled via linearized potential theory. In the lower subdomain, the velocity potential $\Phi^-(x, y, z, t)$ obeys the Laplace equation, Neumann conditions on $z = 0$, and decaying conditions at infinity. When $\Phi_z^-(x, y, 0, t) = (\partial/\partial z)\,\Phi^-(x, y, 0, t)$ is given on the common boundary with the moonpool, Φ^- is obtained everywhere in $z \leqslant 0$ as

$$\Phi^-(x, y, z, t) = \frac{1}{2\pi} \int_0^l \mathrm{d}x' \int_0^b \mathrm{d}y' \frac{\Phi_z^-(x', y', 0, t)}{\sqrt{(x - x')^2 + (y - y')^2 + z^2}}. \tag{1}$$

The matching conditions of the potentials Φ^+ and Φ^- are that they be equal on the common boundary: $\Phi^+(x, y, 0, t) = \Phi^-(x, y, 0, t)$, and their normal derivatives as well: $\Phi_z^+(x, y, 0, t) = \Phi_z^-(x, y, 0, t)$. Hence Φ^+ and Φ_z^+ satisfy the equation

$$\Phi^+(x, y, 0, t) = \frac{1}{2\pi} \int_0^l \mathrm{d}x' \int_0^b \mathrm{d}y' \frac{\Phi_z^+(x', y', 0, t)}{\sqrt{(x - x')^2 + (y - y')^2}}. \tag{2}$$

This is an adequate boundary condition to solve for the flow inside the moonpool, with no longer any need to bother about the lower fluid subdomain. When the draught h is taken as equal to zero, combining equation (2) with the free surface condition readily results in a Fredholm equation for Φ^+ at the free surface. Equations (1) and (2) relate to the three-dimensional problem, which is considered in § 3.

Section 2 is devoted to the two-dimensional case, in a vertical plane in the transverse direction to the barge. Hopefully this is an appropriate simplification to study the piston mode and the transverse sloshing modes when the moonpool is elongated. It is also a problem for which there is abundant literature in the zero draught limit (Henrici, Troesch & Wuytack 1970; Miles 1972; Troesch & Troesch 1972; Troesch 1973; see also Fox & Kuttler 1983). These researchers were considering tanks with lids on the free surface except in a central area, circular or strip-shaped, and they were looking for asymptotic limits of the sloshing frequencies as the walls were taken farther and farther away. As a consequence of there being walls, however remote, there is no mass flux through the aperture. In our case there is a free surface at either side of the barge, so there can be a non-zero mass flux through the moonpool, the most evident manifestation being the piston mode. To mimic the effect of the outer free surface, we locate two sinks symmetrically on the horizontal axis (at keel level), at distances $\pm\lambda B/2$ from the barge centre (B being the beam of the barge and λ some constant larger than 1), so that the total mass flux, at any instant, through the free surface and into the sinks, is zero. Our results become comparable with those of Henrici *et al.*, Miles and Troesch in the limit when λ goes to infinity and h goes to zero.

Eigenfunction expansions are used to solve the boundary value problem inside the moonpool. Favourable comparisons are made with Miles' results in the ($\lambda \to \infty$, $h \to 0$) limit. Natural frequencies of the first sloshing mode and of the piston mode

https://doi.org/10.1017/S0022112000002871 Published online by Cambridge University Press

are given as functions of the draught-to-width ratio h/b, and they are compared with simple analytic expressions, based on so-called single mode approximations. Shapes of the free surface are given for different values of the h/b ratio.

Section 3 is devoted to the three-dimensional case. Again our theory differs from those of Miles and the other investigators in that we allow for a non-zero mass flux through the moonpool. This means that the velocity potential, in the lower half-space, behaves like R^{-1} at infinity, whereas in Miles' case it behaves like R^{-2}. The same technique as in the two-dimensional case is used to set up an eigenvalue problem, the resolution of which gives the natural frequencies and associated eigenvectors. Illustrative results are given for the piston mode and for the first longitudinal and transverse sloshing modes. Single mode approximations are derived that yield the frequencies of the different modes as simple analytic expressions of the two geometric parameters h/l and h/b. A striking result is that the frequencies of the longitudinal sloshing modes increase unboundedly as h/l and b/l both go to zero, the length l being kept constant.

Finally consideration is given to the infinitely long moonpool case, equivalent to a channel in a rigid ice sheet. Given progressive waves with wavenumber k_0 along the channel, an eigenvalue problem is set, that yields their frequency ω_0, the geometric parameters $k_0 b$ and $k_0 h$ being given. It looks as though this problem had never been studied before in infinite water-depth (there is some literature for shallow water, e.g. see Marchenko 1997). Associated shapes of the free surface envelope (in a transverse cut) are given.

2. Two-dimensional case

2.1. *Theory*

Because we will for the moment use complex variables, we take x as the horizontal coordinate and y as the vertical one. The coordinate system is first centred at the middle of the moonpool base, which extends from $x = -b/2$ to $x = b/2$. We first assume the beam of the barge to be infinite. Hence the velocity potential in the lower subdomain $y \leqslant 0$ satisfies the no-flow condition for $|x| > b/2$, $y = 0$, and matching conditions with the velocity potential inside the moonpool for $|x| \leqslant b/2$, $y = 0$. If $\Phi_y^-(x, 0, t)$ is the vertical velocity on this segment, then the complex velocity potential in the lower half-plane is given by

$$f^-(z,t) = -\frac{1}{\pi}\int_{-b/2}^{b/2} \Phi_y^-(\zeta, 0, t)\, \ln(z-\zeta)\, \mathrm{d}\zeta \tag{3}$$

where $z = x + \mathrm{i}\, y$ (see e.g. Newman 1977, ch. 5.7).

As argued in the Introduction this relationship means that, when there is a non-zero mass flux through the moonpool base, the potential (and the pressure) is singular at infinity. This means that our idealization of infinite beam is non-physical. What happens in practice is that the water flows around the keel, up to the free surface (and radiates waves). To model this effect we put two sinks some distance away from the hull, at $x = \pm\lambda B/2 = \pm H/2$, where B is the beam and λ is somewhat larger than 1. The velocity potential in the lower half-plane now is written

$$f^-(z,t) = -\frac{1}{\pi}\int_{-b/2}^{b/2} \Phi_y^-(\zeta, 0, t)[\ln(z-\zeta) - \tfrac{1}{2}\ln(z - H/2) - \tfrac{1}{2}\ln(z + H/2)]\, \mathrm{d}\zeta. \tag{4}$$

https://doi.org/10.1017/S0022112000002871 Published online by Cambridge University Press

Φ^- on the cut $[-b/2\, b/2]$ is given by

$$\Phi^-(x,0,t) = -\frac{1}{\pi}\int_{-b/2}^{b/2} \Phi_y^-(\zeta,0,t)[\ln|x-\zeta| - \tfrac{1}{2}\ln(H/2-x) - \tfrac{1}{2}\ln(H/2+x)]\,\mathrm{d}\zeta$$

or, more simply, with an error $O(b^2/H^2)$

$$\Phi^-(x,0,t) = -\frac{1}{\pi}\int_{-b/2}^{b/2} \Phi_y^-(\zeta,0,t)\,\ln\frac{|x-\zeta|}{H/2}\,\mathrm{d}\zeta. \tag{5}$$

The matching conditions on the cut are that the velocity potentials and their vertical derivatives are equal. Hence Φ^+ inside the moonpool satisfies the boundary condition

$$\Phi^+(x,0,t) = -\frac{1}{\pi}\int_{-b/2}^{b/2} \Phi_y^+(\zeta,0,t)\,\ln\frac{|x-\zeta|}{H/2}\,\mathrm{d}\zeta. \tag{6}$$

We now forget about the lower half-plane and concentrate on the flow within the moonpool. Shifting the coordinate system to the corner, we are looking for the eigen solutions of the boundary value problem

$$\Delta\varphi = 0, \quad 0 \leqslant x \leqslant b, \quad 0 \leqslant y \leqslant h, \tag{7}$$

$$\varphi_x = 0, \quad x = 0, \quad x = b, \tag{8}$$

$$g\,\varphi_y - \omega^2\varphi = 0, \quad y = h, \tag{9}$$

$$\varphi(x,0) = -\frac{1}{\pi}\int_0^b \varphi_y(\zeta,0)\ln\frac{|x-\zeta|}{H/2}\,\mathrm{d}\zeta, \quad y = 0, \tag{10}$$

where

$$\Phi^+(x,y,t) = \mathrm{Re}\,\{\varphi(x,y)\,\mathrm{e}^{-\mathrm{i}\omega t}\}. \tag{11}$$

The domain considered being rectangular in x and y, we look for solutions of the form

$$\varphi(x,y) = A_0 + B_0\,y/h + \sum_{n=1}^{\infty}(A_n\cosh\lambda_n\,y + B_n\sinh\lambda_n\,y)\cos\lambda_n\,x \tag{12}$$

(with $\lambda_n = n\,\pi/b$) so that the Laplace equation and the no-flow conditions on the vertical walls are fulfilled.

The boundary condition on the ficticious bottom gives

$$A_0 + \sum_{n=1}^{\infty} A_n\cos\lambda_n\,x = -\frac{1}{\pi}\int_0^b \left(B_0/h + \sum_{n=1}^{\infty}\lambda_n\,B_n\cos\lambda_n\,\zeta\right)\ln\frac{|x-\zeta|}{H/2}\,\mathrm{d}\zeta.$$

Integrating each side in x from 0 to b gives

$$A_0 = \frac{1}{\pi}\frac{b}{h}B_0\left(\frac{3}{2} + \ln\frac{H}{2b}\right) - \frac{b}{\pi^3}\sum_{n=1}^{\infty}\lambda_n B_n\int_0^{\pi}\int_0^{\pi}\cos n\,v\,\ln|u-v|\,\mathrm{d}u\,\mathrm{d}v. \tag{13}$$

Similarly multiplying both sides with $\cos\lambda_m\,x$ and integrating gives

$$A_m = -\frac{2b}{\pi^3 h}B_0\int_0^{\pi}\int_0^{\pi}\cos mu\,\ln|u-v|\,\mathrm{d}u\,\mathrm{d}v$$

$$-\frac{2b}{\pi^3}\sum_{n=1}^{\infty}\lambda_n B_n\int_0^{\pi}\int_0^{\pi}\cos m\,u\,\cos n\,v\,\ln|u-v|\,\mathrm{d}u\,\mathrm{d}v \tag{14}$$

https://doi.org/10.1017/S0022112000002871 Published online by Cambridge University Press

or, in vector form

$$\boldsymbol{A} = \boldsymbol{AB} \cdot \boldsymbol{B} \tag{15}$$

with $\boldsymbol{A} = (A_0, A_1, \ldots)$, $\boldsymbol{B} = (B_0, B_1, \ldots)$.

Considering then the free surface condition we obtain the following equations

$$\frac{g}{h} B_0 = \omega^2 (A_0 + B_0), \tag{16}$$

$$g\, \lambda_n (A_n \tanh \lambda_n h + B_n) = \omega^2 (A_n + B_n \tanh \lambda_n h), \tag{17}$$

which, upon combination with equation (15), give the eigenvalue problem

$$[\boldsymbol{D}_1 \cdot \boldsymbol{AB} + \boldsymbol{D}_2]\, \boldsymbol{B} = \omega^2\, [\boldsymbol{AB} + \boldsymbol{D}_3]\, \boldsymbol{B} \tag{18}$$

where $\boldsymbol{D}_1, \boldsymbol{D}_2, \boldsymbol{D}_3$ are diagonal matrices.

For numerical resolution this infinite system is truncated to some finite order N. A standard method is then applied to obtain the eigenfrequencies ω_i and eigenvectors $\boldsymbol{B}_i$. Convergence is assessed by repeating the computations for increasing values of the truncation order N.

The numerical evaluation of the integrals that appear in equations (13) and (14) is detailed in the Appendix, § A.1. It turns out (as is obvious from symmetry considerations) that the eigenmodes separate into odd and even modes. The odd modes involve the coefficients A_{2i+1}, B_{2i+1}, the even ones A_{2i}, B_{2i} (i starting from zero). It is only for the even ones that there is a non-zero mass flux through the cut, and that the choice made for H matters.

2.2. *Single mode approximations*

Due to the boundary condition at the bottom, and unlike in a closed rectangular tank, there are couplings, between the different coefficients, expressed by equations (13) and (14). These couplings disappear as the draught h increases with respect to the width b. At small values of h/b, as will be seen, they strongly affect the shape of the free surface, which deviates from a pure sinusoidal function, but affect less the value of the natural frequency. As a result, simple approximations can be derived by retaining, in equations (13), (14), (16), (17), only one couple (A_n, B_n) and setting all the others equal to zero. Then the following expressions are obtained:

Piston mode

In this approximation one assumes the water inside the moonpool to be a solid body. The natural frequency is obtained as

$$\omega_0 \simeq \sqrt{\frac{g}{h + (b/\pi)(\frac{3}{2} + \ln (H/2b))}}. \tag{19}$$

Sloshing modes

One obtains

$$\omega_n^2 \simeq g\, \lambda_n \frac{1 + J_n \tanh \lambda_n h}{J_n + \tanh \lambda_n h} \tag{20}$$

where

$$J_n = -\frac{2n}{b^2} \int_0^b \int_0^b \cos \lambda_n x \cos \lambda_n \zeta \ln |x - \zeta|\, \mathrm{d}x\, \mathrm{d}\zeta = -\frac{2n}{\pi^2} I_{nn},$$

I_{nn} being given in the Appendix, § A.1.

https://doi.org/10.1017/S0022112000002871 Published online by Cambridge University Press

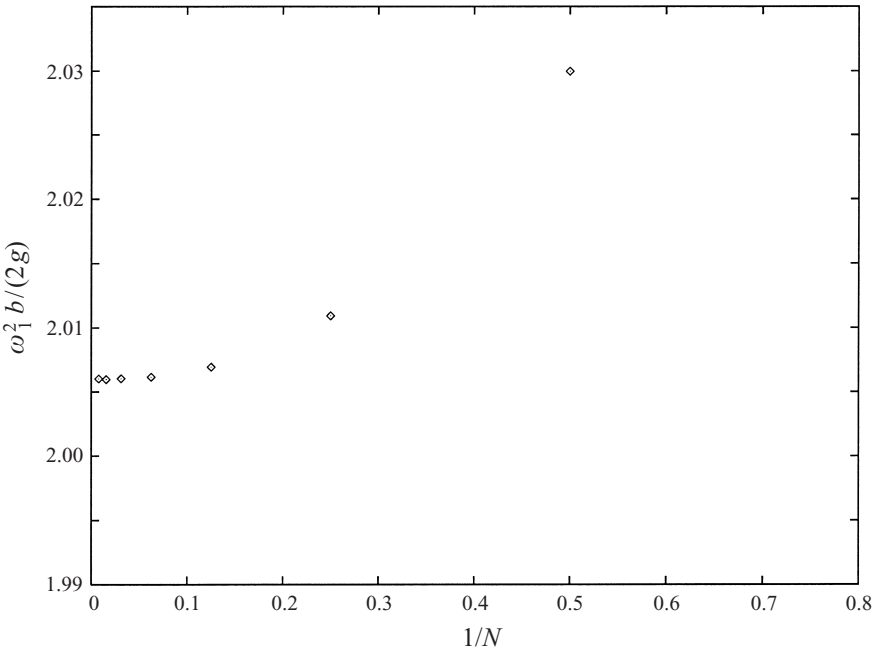


FIGURE 1. Two-dimensional case. Mode 1. $h/b = 0.0001$. Convergence of the natural frequency $\omega_1^2\, b/(2g)$ with respect to the truncation order.

Numerical evaluation gives $J_1 = 0.774$, $J_2 = 0.903$, $J_3 = 0.931$, $J_4 = 0.950$, $J_5 = 0.959$, etc. These values are always less than 1. Hence one can introduce β_n such that

$$J_n = \tanh \beta_n. \tag{21}$$

The frequency is now given by

$$\omega_n^2 \simeq g\, \lambda_n \coth(\lambda_n h + \beta_n). \tag{22}$$

One gets, for the first three modes

$$\omega_1^2 \simeq g\, \frac{\pi}{b} \coth\left(\frac{\pi h}{b} + 1.030\right), \tag{23}$$

$$\omega_2^2 \simeq 2\, g \frac{\pi}{b} \coth\left(\frac{2\pi h}{b} + 1.488\right), \tag{24}$$

$$\omega_3^2 \simeq 3\, g \frac{\pi}{b} \coth\left(\frac{3\pi h}{b} + 1.666\right). \tag{25}$$

2.3. *Results*

We first give some results that illustrate the rate of convergence with respect to the truncation order N of the series. We take a very shallow draught case $h/b = 0.0001$, so we expect to get results in close agreement with the ones given by Miles (1972), who treats the zero draught case. Figure 1 shows the frequency of the first sloshing mode (antisymmetric), in the form $\omega_1^2\, b/(2\, g)$, plotted against $1/N$. For $h = 0$ Miles (1972) obtains 2.006119. Our values converge toward 2.006, which is obtained for $N \geqslant 16$.

https://doi.org/10.1017/S0022112000002871 Published online by Cambridge University Press

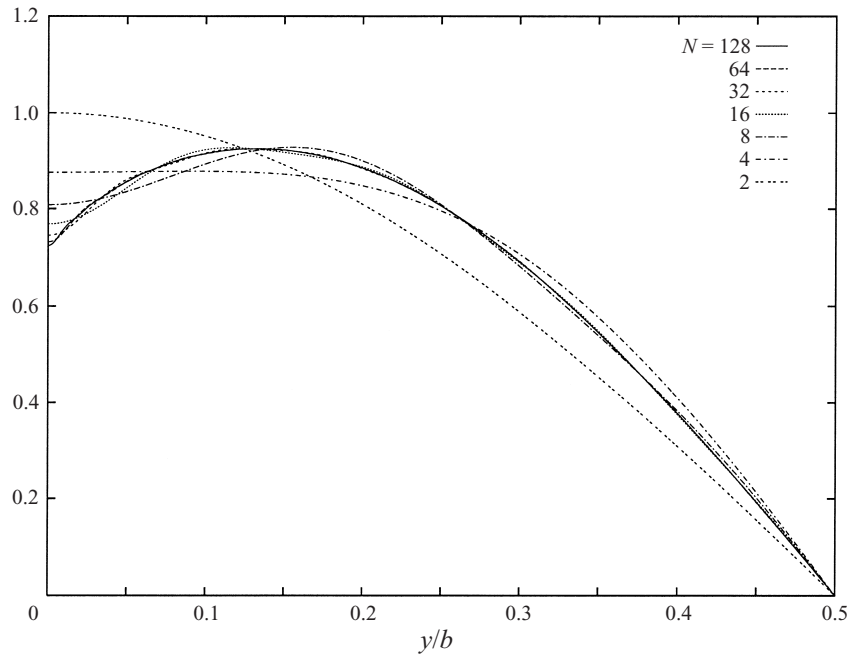


FIGURE 2. Two-dimensional case. Mode 1. $h/b = 0.0001$. Free surface shapes for different truncation orders.

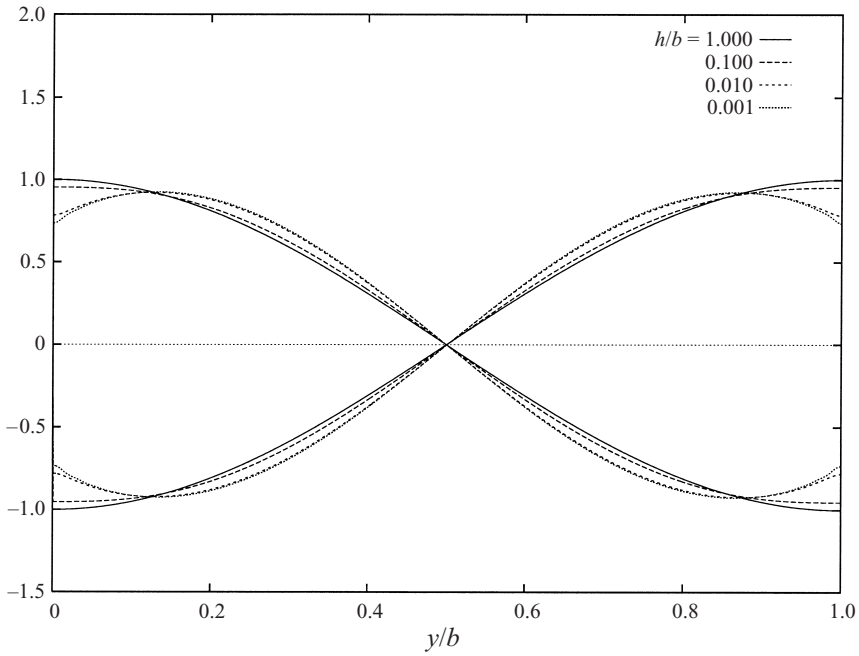


FIGURE 3. Two-dimensional case. Mode 1. Free surface shape for different draught/width ratios.

Figure 2 shows the shape of the free surface in the left-hand half of the moonpool, obtained with different truncation orders. The convergence is slower than for the frequency. This is partly linked to the fact that, in the limit $h/b = 0$, the slope of the free surface at the walls is not zero any more. For larger values of h/b

https://doi.org/10.1017/S0022112000002871 Published online by Cambridge University Press

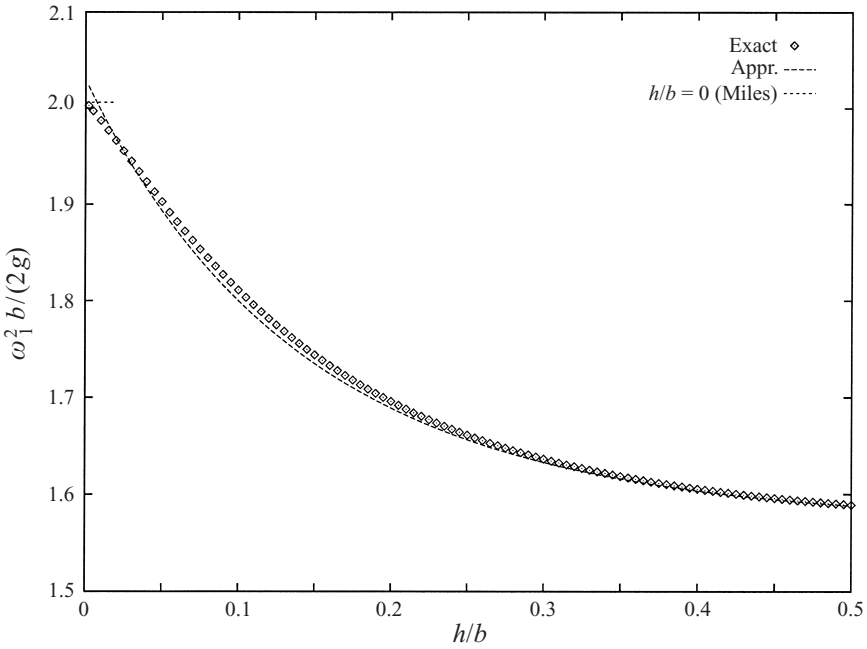


FIGURE 4. Two-dimensional case. Mode 1. Natural frequency $\omega_1^2 b/(2g)$ versus h/b, compared with simple approximation and Miles' asymptotic result.

(say, larger than 0.01), converged shapes are obtained with much lower truncation orders.

Still dealing with the first sloshing mode, we illustrate in figure 3 the effect of varying the draught-to-width ratio, by plotting the free surface profile for $h/b = 1.0$, 0.1, 0.01 and 0.001. A noteworthy result, already visible in figure 2, is that, as h/b decreases to zero, the point of maximum elevation moves away from the wall.

Figure 4 shows the variation of the natural frequency with the h/b ratio, compared to the 'single mode approximation' (23). It can be seen that the agreement is fairly good.

We now consider the mode number 2, which is symmetric and weakly coupled with the piston mode ($m = 0$). To be able to make comparisons with Miles' results we must let H/b go to infinity, and h/b go to zero. This is illustrated in figure 5, which shows the natural frequency of the second mode (still in the form $\omega_2^2 b/(2g)$), for $h/b = 0.0001$, versus $1/\ln(H/b)$. Miles' result is 3.453335. Ours do converge toward 3.453.

Lastly we give some results for the piston mode. This requires making a choice for H/b. The original barge design has a beam (60 m) equal to three times the width of the moonpool. Calculations made with a time domain panel code (Ch. Maisondieu 1999, personal communication) and experiments carried out in the ESIM wave tank have shown that H must be taken as equal to about $1.5B$ for optimized agreement. So we take $H/b = 4.5$.

In figure 6 we show free surface profiles, obtained with $h/b = 1.0$, 0.1, 0.01 and 0.001. As the draught-to-width ratio decreases the free surface becomes bumped in the middle and lower on the sides.

As for the frequency, it turns out that the approximate expression (19) always provides results within less than 1% of the exact values.

https://doi.org/10.1017/S0022112000002871 Published online by Cambridge University Press

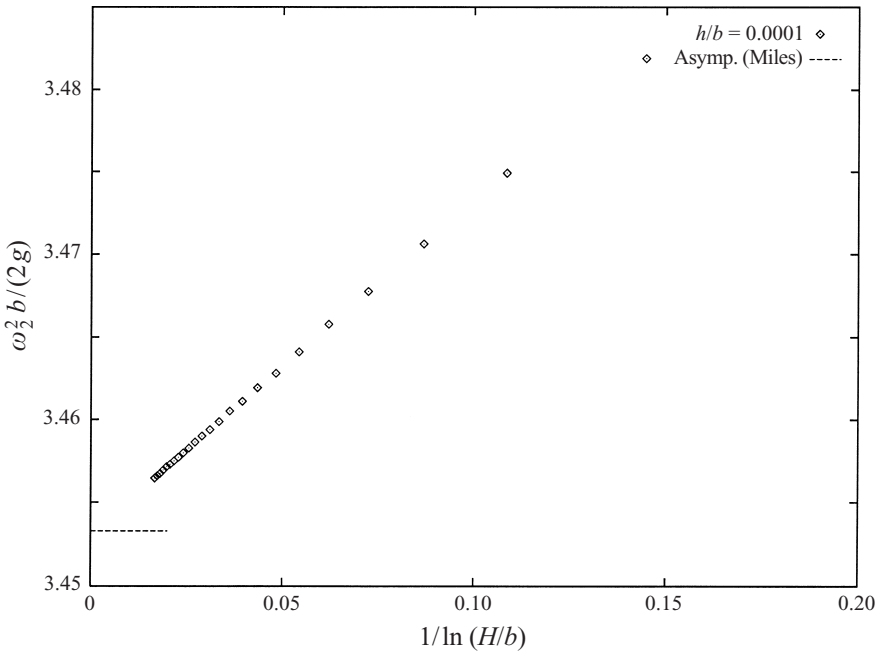


FIGURE 5. Two-dimensional case. Mode 2. Natural frequency $\omega_2^2\, b/(2g)$ versus the position of the two sinks.

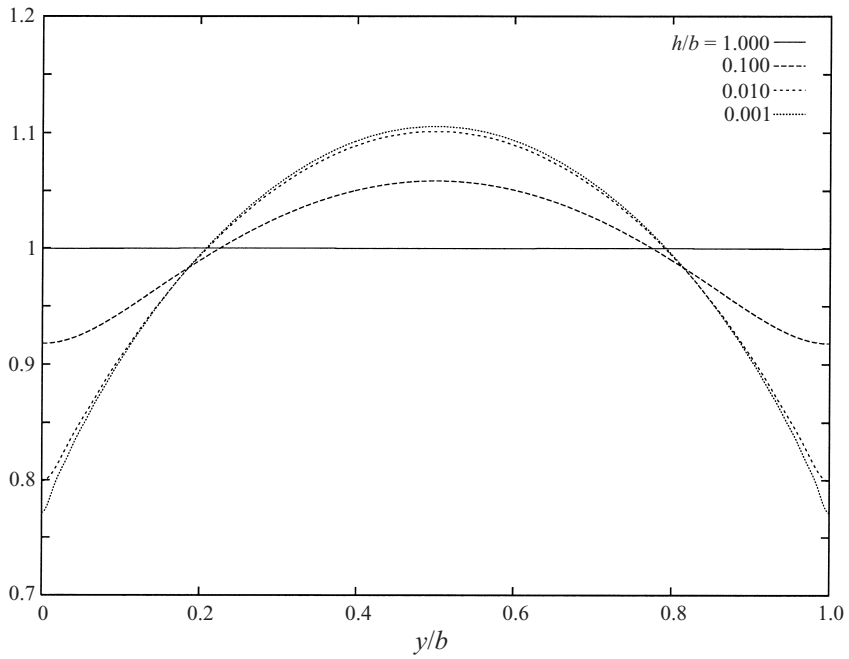


FIGURE 6. Two dimensional case. Piston mode. Free surface profiles for different draught/width ratios.

https://doi.org/10.1017/S0022112000002871 Published online by Cambridge University Press

3. Three-dimensional case

3.1. *Theory*

We now proceed to the three-dimensional case of a rectangular moonpool with length l, width b and draught h. We assume the beam and length of the barge to be infinite, the barge being motionless, so that, as argued in the Introduction, the velocity potential Φ^+ inside the moonpool satisfies the boundary condition at $z = 0$

$$\Phi^+(x, y, 0, t) = \frac{1}{2\pi} \int_0^l \mathrm{d}x' \int_0^b \mathrm{d}y' \frac{\Phi_z^+(x', y', 0, t)}{\sqrt{(x - x')^2 + (y - y')^2}} \tag{2}$$

(the coordinate system being centred at one of the lower corners).

Unlike with the two-dimensional case there is no problem of the pressure being singular at infinity.

We follow the same resolution method as in the two-dimensional case. We look for Φ^+ in the form

$$\Phi^+(x, y, z, t) = \mathrm{Re}\left\{\varphi(x, y, z)\, \mathrm{e}^{-\mathrm{i}\omega t}\right\}$$

$$\varphi = \sum_{n=0}^{\infty} \sum_{q=0}^{\infty} \cos \lambda_n x \, \cos \mu_q y \, (A_{nq} \cosh \nu_{nq} z + B_{nq} \sinh \nu_{nq} z) \tag{26}$$

where $\lambda_n = n\pi/l$, $\mu_q = q\pi/b$, $\nu_{nq}^2 = \lambda_n^2 + \mu_q^2$, and, when $n = q = 0$, the hyperbolic functions are replaced with $A_{00} + B_{00} z/h$.

The Laplace equation and the no-flow conditions at the vertical walls are fulfilled. There only remains the bottom boundary condition (2) and the free surface equation (9).

We use the same Galerkin procedure: we insert (26) into the bottom boundary condition, multiply each side with $\cos \lambda_m x \cos \mu_p y$ and integrate in x and y over the bottom. This procedure requires the evaluation of the integrals

$$I_{mnpq} = \int_0^l \mathrm{d}x \int_0^l \mathrm{d}x' \int_0^b \mathrm{d}y \int_0^b \mathrm{d}y' \, \frac{\cos \lambda_m x \, \cos \lambda_n x' \, \cos \mu_p y \, \cos \mu_q y'}{\sqrt{(x - x')^2 + (y - y')^2}} \tag{27}$$

which is presented in the Appendix, § A.2.

It turns out, again as expected from geometric considerations, that I_{mnpq} is non-zero only when both $m + n$ and $p + q$ are even. This means that four types of resonant modes can appear:

(i) m, n, p, q all even: the modes are symmetric both in x and y. This is the case of the piston mode.

(ii) m and n odd, p and q even: the modes are antisymmetric in x and symmetric in y. This is the case of the longitudinal sloshing modes.

(iii) m and n even, p and q odd: this is the same as case (ii) with the x and y coordinates interchanged. This is the case of the transverse sloshing modes.

(iv) m, n, p, q all odd: the modes are antisymmetric both in x and y. They can be excited by the yaw motion of the barge. They have not been considered in this analysis.

Since the numerical evaluation of the I_{mnpq} coefficients is somewhat time consuming, and the size of the final system can be quite large, the two cases n and q both even, n odd and q even, have been separated from the start in the resolution, which follows closely the two-dimensional one (so it is no longer detailed here).

https://doi.org/10.1017/S0022112000002871 Published online by Cambridge University Press

3.2. *Single mode approximations*

When truncation orders N and Q have been specified, the eigenvalue problem can be exactly solved and the natural frequencies are obtained. As in the two-dimensional case, it turns out that good approximations of these frequencies are obtained when only one term of the development is retained: $n = q = 0$ for the piston mode, $n = 1$ (or 2, 3, etc.), $q = 0$ for the longitudinal sloshing modes. Simple expressions can then be derived.

Piston mode

Again this approximation means that we simulate the water inside the moonpool as a solid body. The following expression is obtained for the natural frequency:

$$\omega_{00} \simeq \sqrt{\frac{g}{h + b\, f_3(b/l)}} \tag{28}$$

where

$$f_3 = \frac{1}{\pi}\left\{\sinh^{-1}\left(\frac{l}{b}\right) + \frac{l}{b}\sinh^{-1}\left(\frac{b}{l}\right) + \frac{1}{3}\left(\frac{b}{l} + \frac{l^2}{b^2}\right) - \frac{1}{3}\left(1 + \frac{l^2}{b^2}\right)\sqrt{\frac{b^2}{l^2} + 1}\right\} \tag{29}$$

(see the Appendix, § A.2.1).

The quantity $\rho\, b^2\, l\, f_3(b/l)$ can be interpreted as the zero-frequency limit of the heave added mass of a flat plate of length l and breadth b at the free surface. As l increases to infinity, b and h being kept constant, f_3 also increases to infinity and the frequency becomes nil. So the two-dimensional situation is asymptotically recovered: there can be no piston mode in two dimensions unless some tricks are applied to simulate the outer free surface.

Longitudinal sloshing modes

One obtains the same kind of expression as in two dimensions:

$$\omega_{n0}^2 \simeq g\, \lambda_n \frac{1 + J_{n0}\, \tanh \lambda_n h}{J_{n0} + \tanh \lambda_n h} \tag{30}$$

where

$$J_{n0} = \frac{n}{b\, l^2}\int_0^b \mathrm{d}y \int_0^b \mathrm{d}y' \int_0^l \mathrm{d}x \int_0^l \mathrm{d}x' \frac{\cos \lambda_n x \cos \lambda_n x'}{\sqrt{(x - x')^2 + (y - y')^2}} = \frac{n}{b\, l^2}\, I_{nn00}.$$

J_{n0} can be expressed as (see the Appendix, § A.2.2)

$$J_{n0} = \frac{2}{n\, \pi^2\, r}\left\{\int_0^1 \frac{r^2}{u^2\sqrt{u^2 + r^2}}\left[1 + (u - 1)\cos(n\pi u) - \frac{\sin(n\,\pi\, u)}{n\,\pi}\right]\mathrm{d}u + \frac{1}{\sin\theta_0} - 1\right\} \tag{31}$$

where $r = b/l$ and $\tan\theta_0 = r^{-1}$.

Figure 7 shows J_{n0}, versus $\lambda_n\, b = n\,\pi\, b/l$, for $n = 1, 2, 4, 10$. It appears again that J_{n0} is always less than 1 (and it can be checked, at least numerically, that when $\lambda_n b$ goes to infinity, the two-dimensional J_n functions are recovered). Hence one can introduce β_{n0} such that

$$J_{n0} = \tanh \beta_{n0}$$

https://doi.org/10.1017/S0022112000002871 Published online by Cambridge University Press

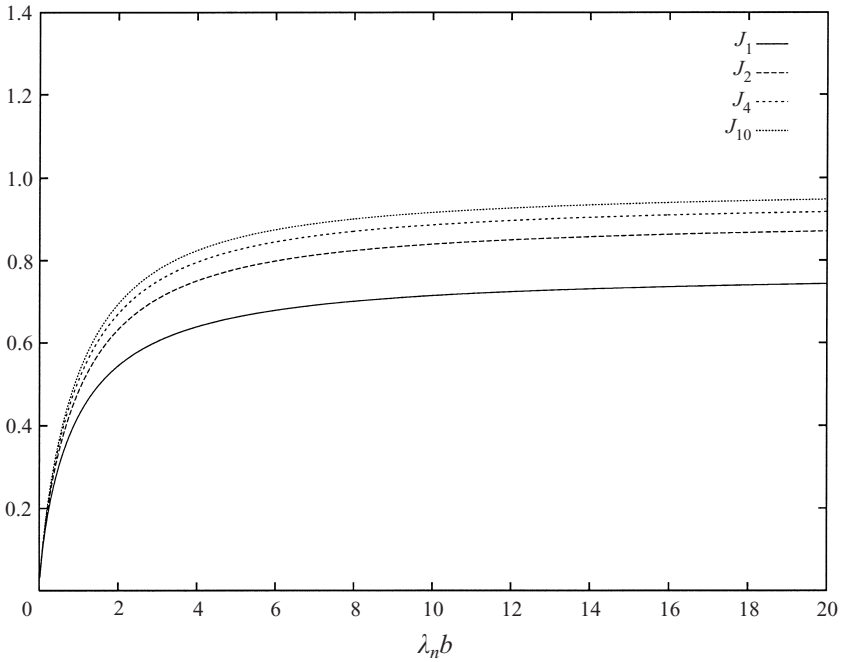


FIGURE 7. Three-dimensional case. Longitudinal sloshing modes. Functions $J_{n0}(\lambda_n b)$ for $n = 1$, 2, 4 and 10.

which leads to the dispersion equation

$$\omega_{n0}^2 \simeq g\,\lambda_n \coth\left[\lambda_n h + \beta_{n0}(\lambda_n b)\right]. \tag{32}$$

From figure 7 it appears that, when $\lambda_n b$ goes to zero, so do J_{n0} and β_{n0}. Hence very high values of ω_{n0} can be obtained when both the draught h and the breadth b are small compared to the length l of the moonpool.

Another result that is readily obtained from the approximations (28) and (32) is that the natural frequency of the piston mode is always less than the frequency of the first sloshing mode, whatever the length, width and draught of the moonpool.

3.3. *Results*

It is impractical to try to give results for all the ranges of the geometric parameters l/b and h/b. Therefore we select three values of the 'aspect ratio' l/b of the moonpool: $l/b = 1$, $l/b = 4$ (the original barge case) and $l/b = 16$, and we vary h/b from 0 to 1.

First we give results for the natural frequency of the piston mode. They are shown in figure 8, where $\omega_{00}^2\, h/g$ is given as a function of h/b, for the three aspect ratios l/b, according to the approximation (28) and after solving the eigenvalue problem. The truncation orders N and Q of the double series are given in the figure. It can be observed, again, that the two sets of values agree closely. The natural frequency is lowest for the most elongated moonpool, due to the increase of the added mass coefficient f_3 with the aspect ratio l/b.

Figure 9 gives similar results for the first longitudinal sloshing mode, with the difference that the frequency ω_{10} is given in the form $\omega_{10}^2\, l/(\pi g)$ which has an asymptotic value of one as h/l or b/l increases. The agreement between the approximate values provided by equation (32) and the exact ones is rather good, except at the very low values of h/b, for the most elongated moonpool. In this latter case, the parameter

https://doi.org/10.1017/S0022112000002871 Published online by Cambridge University Press

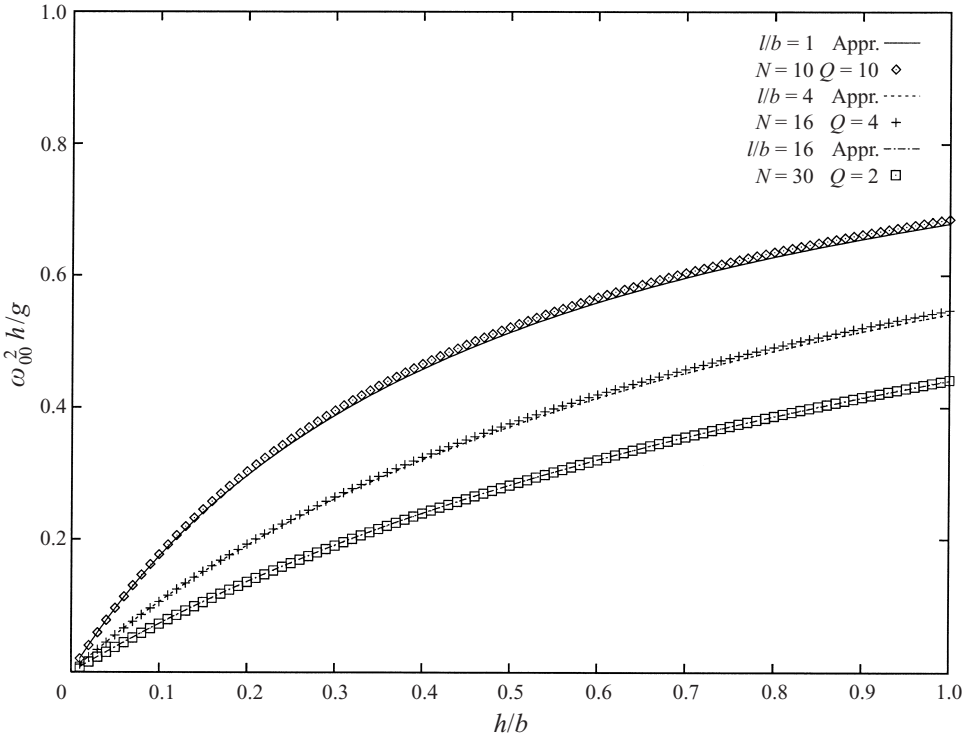


FIGURE 8. Three-dimensional case. Piston mode. Natural frequency $\omega_{00}^2\, h/g$ versus h/b for three l/b ratios.

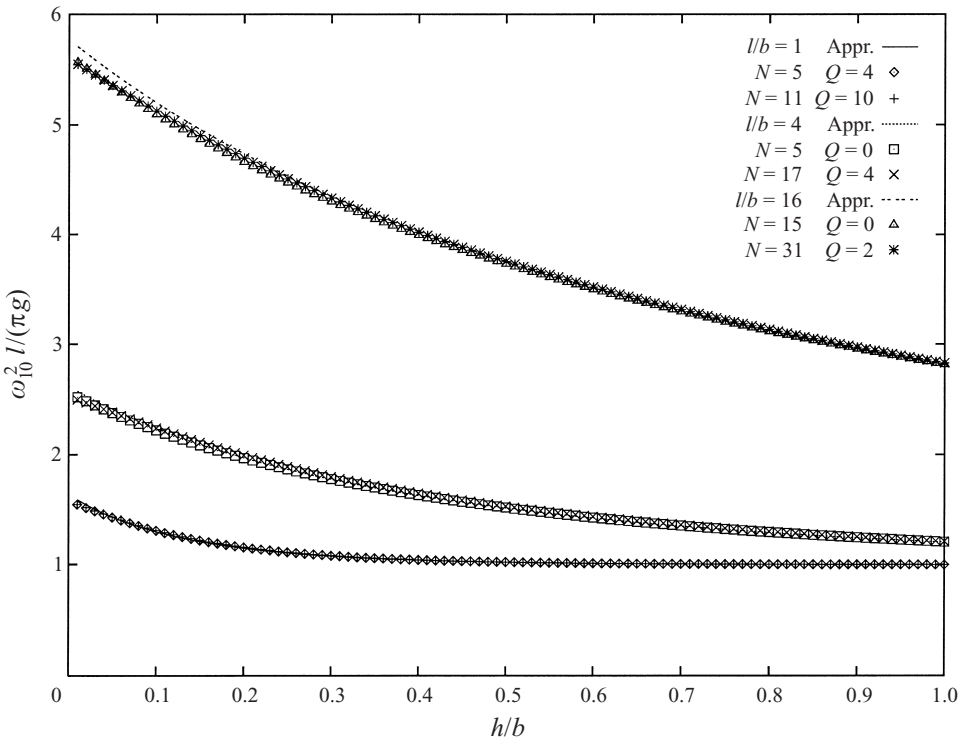


FIGURE 9. Three-dimensional case. First longitudinal sloshing mode. Natural frequency $\omega_{10}^2\, l/(\pi g)$ versus h/b for three l/b ratios.

https://doi.org/10.1017/S0022112000002871 Published online by Cambridge University Press

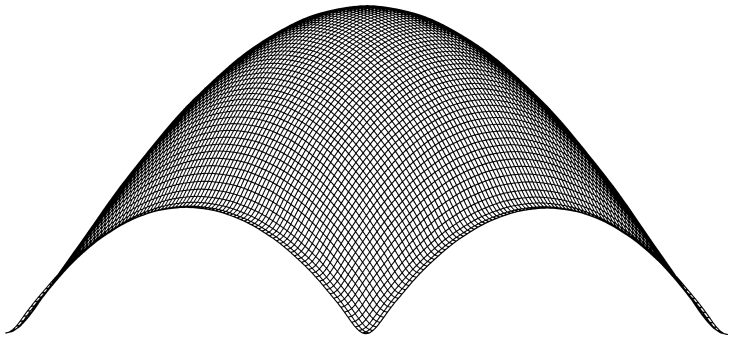


FIGURE 10. Three-dimensional case. Piston mode. Free surface shape for $l = b = 40h$.

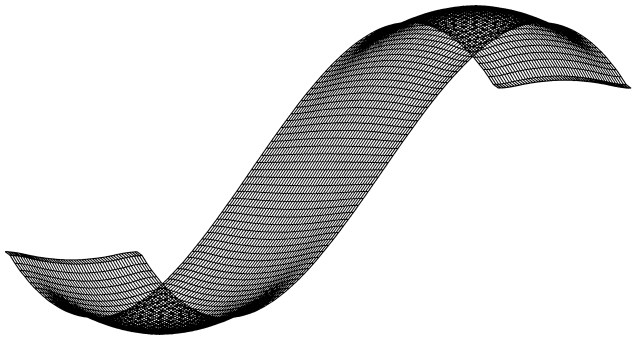


FIGURE 11. Three-dimensional case. First longitudinal sloshing mode. Free surface shape for $l = 160h$, $b = 10h$.

$\omega_{10}^2 l/(\pi g)$ reaches values as high as 5.6, meaning a natural frequency 2.4 times higher than the deep draught (or large width) limit.

The following figures provide some three-dimensional views of the free surface at resonance, the draught h being taken as $h = \sqrt{b\,l}/40$. This shallow case is chosen to enhance the deviations from pure sinusoidal shapes (or flat shapes, in the case of the piston mode), while convergence can still be attained at not too high values of the truncation orders N and Q.

Figure 10 shows the piston mode in the square moonpool. To obtain this shape the double series was truncated at $N = Q = 22$. The maximum elevation, in the middle, is 1.23. The minimum elevation is 0.66, in the corners. These values relate to an average of one over the moonpool.

Figure 11 shows the first longitudinal sloshing mode in the most elongated moonpool. The double series was truncated at $N = 63$ and $Q = 6$. Because of lateral confinement the free surface is nearly straight in the transverse direction. But it is quite distorted longitudinally: deviations from a pure sinusoidal shape are actually greater than what the two-dimensional analysis would yield for a moonpool of same length over height ratio.

Finally, in the intermediate moonpool, figure 12 shows the first transverse sloshing mode (obtained with $N = 10$ and $Q = 35$). It can be observed that the amplitude of the sloshing motion varies strongly along the length. In the centre it is about 3.5 greater than at the endwalls! This means that a two-dimensional approach is not altogether appropriate to study the transverse sloshing modes: it provides the correct frequency but it cannot give the amplitude.

https://doi.org/10.1017/S0022112000002871 Published online by Cambridge University Press

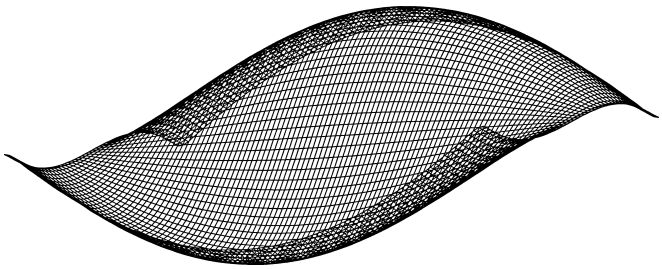


FIGURE 12. Three-dimensional case. First transverse sloshing mode. Free surface shape for $l = 80h$, $b = 20h$.

4. The dispersion equation for progressive waves in a channel through an ice sheet

We now move on to the simpler case of a moonpool with no endwalls, equivalent to a channel through a rigid ice sheet. We consider progressive waves travelling along the channel, with wavenumber k_0, and we seek to express their frequency. We apply the same method as in the finite moonpool case, the only difference being that we start from the expression, for the velocity potential inside the channel,

$$\varphi(x, y, z) = \mathrm{e}^{\mathrm{i}k_0 x} \sum_{n=0}^{N} \cos \mu_n y \, (A_n \cosh \nu_n z + B_n \sinh \nu_n z), \tag{33}$$

with

$$\Phi^+(x, y, z, t) = \mathrm{Re}\,\{\varphi(x, y, z)\,\mathrm{e}^{-\mathrm{i}\omega t}\}.$$

Here $\mu_n = n\pi/b$, $\nu_n^2 = k_0^2 + \mu_n^2$. Only even values of n are retained, since we are only interested in symmetric solutions.

The same boundary condition (2) applies at $z = 0$, giving

$$\mathrm{e}^{\mathrm{i}k_0 x} \sum_n \cos \mu_n y \, A_n = \frac{1}{2\pi} \int_{-\infty}^{\infty} \mathrm{d}x' \int_0^b \mathrm{e}^{\mathrm{i}k_0 x'} \frac{\sum_n \nu_n \cos \mu_n y' B_n}{\sqrt{(x - x')^2 + (y - y')^2}} \, \mathrm{d}y'$$

or, setting $x' = x + u$:

$$\sum_n \cos \mu_n y \, A_n = \frac{1}{2\pi} \int_{-\infty}^{\infty} \mathrm{d}u \int_0^b \mathrm{e}^{\mathrm{i}k_0 u} \frac{\sum_n \nu_n \cos \mu_n y' B_n}{\sqrt{u^2 + (y - y')^2}} \, \mathrm{d}y'. \tag{34}$$

Multiplying both sides with $\cos \mu_m y$ and integrating in y from 0 to b gives

$$A_m = \frac{1}{\pi b(1 + \delta_{m0})} \sum_n \nu_n B_n \tilde{I}_{mn} \tag{35}$$

with

$$\tilde{I}_{mn} = \int_{-\infty}^{\infty} \mathrm{d}u \int_0^b \mathrm{d}y \int_0^b \mathrm{d}y' \, \mathrm{e}^{\mathrm{i}k_0 u} \frac{\cos \mu_m y \cos \mu_n y'}{\sqrt{u^2 + (y - y')^2}}. \tag{36}$$

The calculation of $\tilde{I}_{mn}$ is given in the Appendix, § A.3.

Again, together with the free surface condition, an eigenvalue problem can be set to obtain the frequencies ω_n and associated free surface shapes. The case when A_0 and B_0 are dominant over the other coefficients corresponds to waves travelling along the channel, the other cases to waves that are both progressive and reflecting on the sides. We are not interested in the latter and we only consider the inline case.

https://doi.org/10.1017/S0022112000002871 Published online by Cambridge University Press

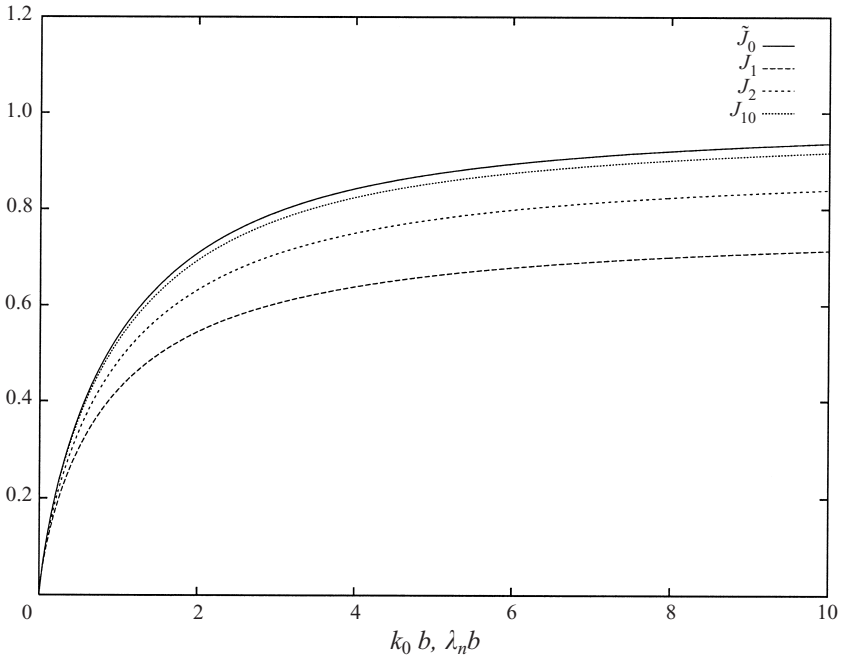


FIGURE 13. Channel through the ice sheet. Function $\tilde{J}_0(k_0\,b)$ compared with the functions $J_{n0}(\lambda_n\,b)$.

Most likely, as in the longitudinally restricted case, a good approximation of the frequency ω_0 of the inline mode can be obtained by retaining only A_0 and B_0, setting all other coefficients equal to zero. We get

$$\omega_0^2 \simeq g\,k_0 \frac{1+\tilde{J}_0 \tanh k_0 h}{\tilde{J}_0 + \tanh k_0 h}$$

where

$$\tilde{J}_0(k_0 b) = \frac{k_0 b}{2\pi}\int_{-\infty}^{\infty} \mathrm{d}u \int_0^1 \mathrm{d}y \int_0^1 \mathrm{d}y' \frac{\mathrm{e}^{\mathrm{i}\,k_0 b\,u}}{\sqrt{u^2+(y-y')^2}} = \frac{k_0}{2\pi b}\,\tilde{I}_{00}. \tag{37}$$

It is shown in the Appendix, § A.3 that $\tilde{J}_0(k_0 b)$ can be evaluated as

$$\tilde{J}_0(k_0 b) = 1 - \frac{2}{\pi\,k_0 b}\left(1 - \int_0^1 \mathrm{e}^{-k_0 b\,(1-u^2)^{-1/2}}\,\mathrm{d}u\right). \tag{38}$$

$\tilde{J}_0$ is shown in figure 13, together with the functions $J_{n0}, n = 1, 2, 10$, derived in § 2. It turns out to be the limiting case of $J_{n0}(\lambda_n b)$ when n goes to infinity. The approximate dispersion equation can again be put in the form

$$\omega_0^2 \simeq g\,k_0 \coth[k_0\,h + \tilde{\beta}_0(k_0\,b)] \tag{39}$$

where $\tilde{J}_0(k_0 b) = \tanh(\tilde{\beta}_0)$.

To present results we first select three draught-to-width ratios: $h/b = 0.01$, $h/b = 0.10$, $h/b = 1.00$, and we vary $k_0\,b$ from 0 to 5. The natural frequency is obtained by solving the eigenvalue problem (with a truncation order N equal to 40), and by using the approximation (39). Figure 14 shows the results obtained, the frequency being given in the form $\sqrt{g\,k_0}/\omega_0$: it is the ratio of the phase velocity of the waves in an

https://doi.org/10.1017/S0022112000002871 Published online by Cambridge University Press

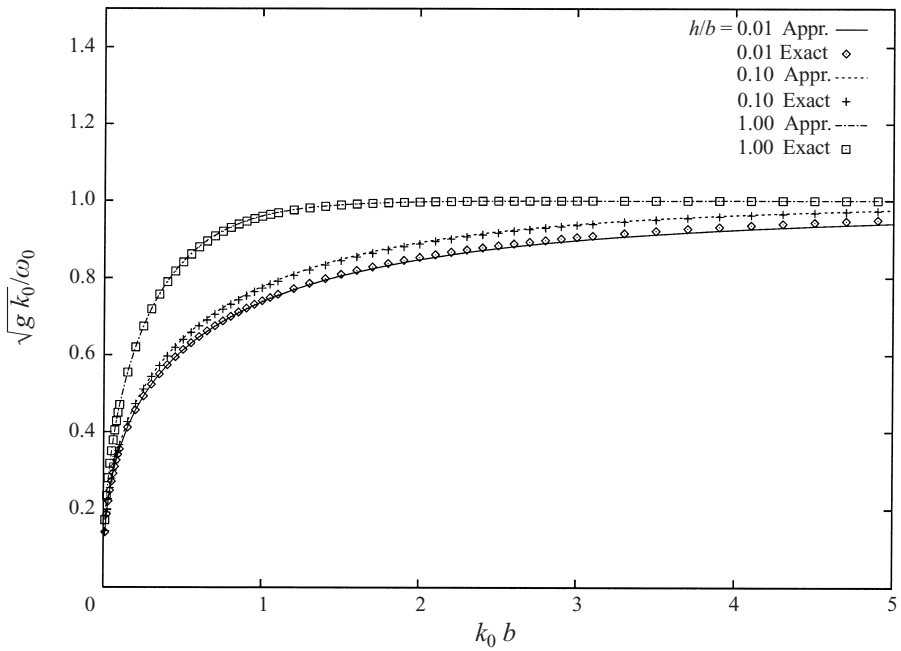


FIGURE 14. Channel through the ice sheet. Dispersion equation. $\sqrt{g\,k_0}/\omega_0$ as a function of $k_0\,b$ for different draught-to-width ratios.

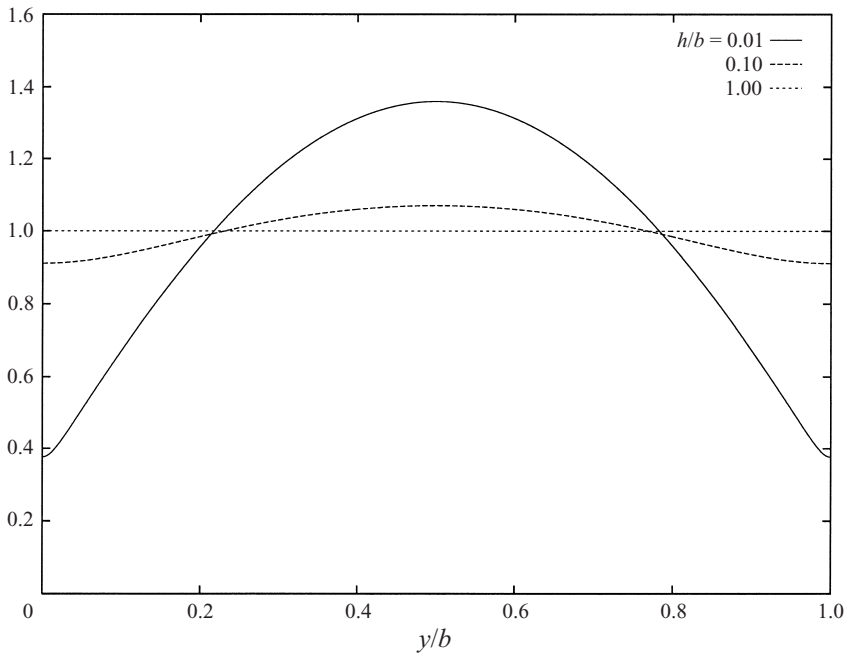


FIGURE 15. Channel through the ice sheet. Transverse cuts of the free surface envelope for $k_0\,b = 10$ and different h/b ratios.

unbounded ocean to the phase velocity of the waves inside the channel. When the wavelength becomes large compared both to the width b and to the draught h, the phase velocity ratio goes to zero, meaning that the waves in the channel travel faster and faster. From the figure it can also be observed that the agreement between the

https://doi.org/10.1017/S0022112000002871 Published online by Cambridge University Press

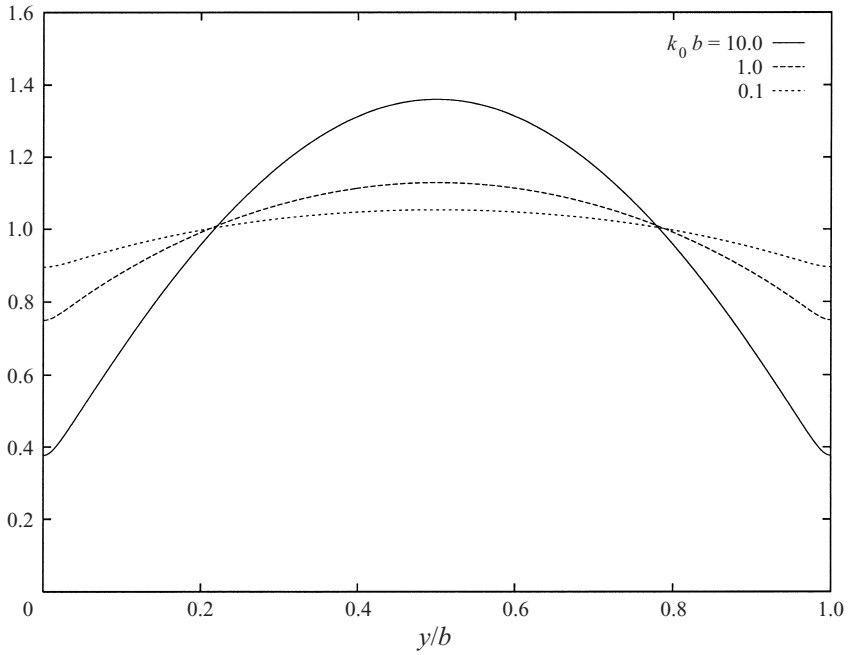


FIGURE 16. Channel through the ice sheet. Transverse cuts of the free surface envelope for $h/b = 0.01$ and different $k_0\,b$ values.

approximate dispersion equation and the exact one is quite good, except for a very slight deviation when h/b is very small and $k_0 b$ is large.

We finally present results for the free surface profile. The linear system giving the A_n and B_n coefficients is real, so the complex A_n and B_n coefficients have the same arguments. This means that the wave crests remain straight, perpendicular to the x-axis.

Figure 15 shows transverse cuts of the free surface envelope, obtained for $k_0\,b = 10$ and the same values of h/b as in the previous figure. The truncation order has been moved up to 80. At $h = b$, as expected, the envelope profile is a straight line: the wave amplitude is constant over the width. At $h/b = 0.10$ there is a weak modulation of the amplitude. At $h/b = 0.01$, the wave amplitude gets much larger at the centreline (nearly 1.4 times the average value) while it drops to less than 0.4 the average value along the walls.

Finally figure 16 shows similar cuts for three different values of $k_0\,b$ (10, 1 and 0.1), while the ratio h/b is kept constant at 0.01. The amplitude modulation along the cut is greatest for the shortest waves.

5. Discussion and conclusion

The most remarkable result obtained in this analysis is the increase in frequency of the longitudinal sloshing modes as the width and draught of the moonpool become smaller. This phenomenon is associated with the fluid motion that takes place beneath the hull. An interpretation, based on energy considerations, is as follows.

Let us first consider a closed rectangular tank with finite depth h. According to linearized potential flow theory, the free surface elevation associated with the sloshing

https://doi.org/10.1017/S0022112000002871 Published online by Cambridge University Press

mode n is

$$\eta = A \cos \lambda_n x \, \cos \omega_n t \tag{40}$$

where $\lambda_n = n\pi/l$, $\omega_n^2 = g\lambda_n \tanh \lambda_n h$.

The velocity potential is

$$\Phi(x, y, z, t) = -\frac{A\, g}{\omega_n} \frac{\cosh \lambda_n z}{\cosh \lambda_n h} \cos \lambda_n x \, \sin \omega_n t \tag{41}$$

and the longitudinal and vertical components of the fluid velocity:

$$u = A \sqrt{g\, \lambda_n} \sqrt{\coth \lambda_n h} \frac{\cosh \lambda_n z}{\cosh \lambda_n h} \, \sin \lambda_n x \, \sin \omega_n t, \tag{42}$$

$$w = -A \sqrt{g\, \lambda_n} \sqrt{\tanh \lambda_n h} \frac{\sinh \lambda_n z}{\sinh \lambda_n h} \, \cos \lambda_n x \, \sin \omega_n t. \tag{43}$$

The potential and kinetic energies are given by

$$E_P = \frac{1}{2} \rho\, g \iint_{S_F} \eta^2 \, \mathrm{d}S = \frac{1}{2\, g} \rho \iint_{S_F} \Phi_t^2 \, \mathrm{d}S, \tag{44}$$

$$E_K = \frac{1}{2} \rho \iiint_V (\nabla \Phi)^2 \, \mathrm{d}V = \frac{1}{2} \rho \iint_{S_F} \Phi \, \Phi_z \, \mathrm{d}S = -\frac{1}{2\, g} \rho \iint_{S_F} \Phi \, \Phi_{tt} \, \mathrm{d}S \tag{45}$$

where V is the fluid domain and S_F the mean free surface $z = h$.

As a result the potential and kinetic energies are independent of the depth h:

$$E_P = \tfrac{1}{4} \rho\, g\, b\, l\, A^2 \, \cos^2 \omega_n t, \tag{46}$$

$$E_K = \tfrac{1}{4} \rho\, g\, b\, l\, A^2 \, \sin^2 \omega_n t \tag{47}$$

(so that the total energy remains constant).

When the depth h decreases there is less fluid to participate in the kinetic energy and, moreover, the vertical component of the velocity, given by (43), becomes smaller by the factor $\sqrt{\tanh \lambda_n h}$, due to the decrease of the frequency ω_n. However the horizontal motion of the fluid particles increases by the factor $\coth \lambda_n h$, and hence the horizontal velocity by the factor $\sqrt{\coth \lambda_n h}$, so that the kinetic energy is maintained. It is quite remarkable that the increase of the horizontal velocity is associated with a decrease of the frequency.

In the moonpool case equations (44)–(47) giving the potential and kinetic energies still hold, under the 'single mode approximation'. But there is now, in the small draught and small width case, too much fluid to participate in the kinetic energy, because of the additional fluid region beneath the hull. The way to preserve the energy balance now is to reduce the horizontal component of the velocity, by the factor $\sqrt{\tanh (\lambda_n h + \beta_{n0})}$, with the associated result that the frequency increases.

In fact the single mode approximation means that the velocity potential of the sloshing flow, inside the moonpool, is given by

$$\Phi_{n0}^{+}(x, y, z, t) \simeq -\frac{A_{n0}\, g}{\omega_{n0}} \frac{\sinh (\lambda_n z + \beta_{n0})}{\sinh (\lambda_n h + \beta_{n0})} \cos \lambda_n x \, \sin \omega_{n0} t. \tag{48}$$

Similar effects are found with the waves travelling in the ice-channel. The horizontal component of the fluid particle motion decreases compared with the vertical one and

https://doi.org/10.1017/S0022112000002871 Published online by Cambridge University Press

the velocity potential of the flow within the channel is approximately given by

$$\Phi^+(x,y,z,t) = \frac{A\,g}{\omega_0}\,\frac{\sinh(k_0\,z+\tilde{\beta}_0)}{\sinh(k_0\,h+\tilde{\beta}_0)}\sin(k_0\,x-\omega_0\,t). \tag{49}$$

In this case we have obtained that the crest lines remain straight, because we have assumed the channel to be infinitely long. One may wonder what would happen at the mouth of the channel as the wave system propagates into it. Most probably the waves would be accelerated along its edges and the crest lines would first bend.

A related problem that would be worth considering is the floating dock, where the waves travelling along its edges should also lengthen, with the result that the crest lines would bend and that the wave energy flux would tend to diverge away from the edges.

Finally some mention should be made of the relevance of all these results for the original problem, of a barge of finite beam and length with a moonpool inside. In the designs considered, the beam is about three times the moonpool width and the length of the barge varies from two to four times the length of the moonpool, so it may be questioned whether the infinite beam and length assumption is applicable. The natural frequencies of the piston and antisymmetric sloshing modes appear very precisely as peaks in the damping coefficients calculated with diffraction radiation codes. They were found to agree very well with the values delivered by the simple formulae (28) and (32), which are therefore quite helpful for engineering studies.

The author is grateful to D. V. Evans who brought to his attention the works of B. A. Troesch and of his coworkers, and of J. W. Miles. This work was partly carried out within an industrial project, led by Bouygues Offshore. Other partners in the project are Elf E. P., IFP, Ifremer, Principia and Sedco Forex.

Appendix A. Evaluation of integrals

A.1. *Two-dimensional case*

The integral

$$I_{mn} = \int_0^\pi \mathrm{d}u \int_0^\pi \mathrm{d}v\,\cos mu\,\cos nv\,\ln|u-v|$$

needs to be evaluated, where m and n are integers, at least one of them non-zero.

Making use of

$$\ln|u-v| = \lim_{\epsilon\to 0}\left[\ln\epsilon + \int_0^\infty \frac{\mathrm{d}k}{k}\,\mathrm{e}^{-k\,\epsilon}\,[1-\cos k\,(u-v)]\right],$$

the u and v integrations are easily performed, then ϵ is set equal to zero, to obtain

$$I_{mn} = -2\int_0^\infty \frac{k\,[1-(-1)^m\,\cos k\pi]}{(k^2-m^2)\,(k^2-n^2)}\,\mathrm{d}k$$

for $m+n$ even and $I_{mn}=0$ for $m+n$ odd.

This expression can be transformed by integration around the first quadrant of the complex plane, along the positive real semi-axis (with indentations around the two poles), one quarter of a remote circle, and back to the origin along the positive imaginary semi-axis, to obtain

$$I_{mn} = \frac{2}{m^2-n^2}\,(\ln m-\ln n) - 2\,(-1)^m\int_0^\infty \frac{y\,\mathrm{e}^{-\pi\,y}}{(y^2+m^2)\,(y^2+n^2)}\,\mathrm{d}y \quad \text{for } m\neq n\ \ m,\ n\neq 0,$$

https://doi.org/10.1017/S0022112000002871 Published online by Cambridge University Press

$$I_{m0} = 2\int_0^1 \frac{1-\mathrm{e}^{-\pi y}}{y\,(y^2+m^2)}\,\mathrm{d}y - 2\int_1^\infty \frac{\mathrm{e}^{-\pi y}}{y\,(y^2+m^2)}\,\mathrm{d}y + \frac{1}{m^2}\,\ln(1+m^2) \quad \text{for } n=0,$$

$$I_{mm} = \frac{1}{m^2}\,[1-(-1)^m] - \frac{\pi^2}{2\,m} + (-1)^m\,\pi\int_0^\infty \frac{\mathrm{e}^{-\pi y}}{y^2+m^2}\,\mathrm{d}y \quad \text{for } n=m.$$

A.2. *Three-dimensional case*

The integral

$$I_{mnpq} = \int_0^l \mathrm{d}x \int_0^l \mathrm{d}x' \int_0^b \mathrm{d}y \int_0^b \mathrm{d}y' \,\frac{\cos\lambda_m x\,\cos\lambda_n x'\,\cos\mu_p y\,\cos\mu_q y'}{\sqrt{(x-x')^2+(y-y')^2}}$$

needs to be evaluated.

A.2.1. *Case* $m=n=p=q=0$

For this case

$$I_{0000} = \iint_S \iint_S \frac{1}{PQ}\,\mathrm{d}S_P\,\mathrm{d}S_Q.$$

Making use of the identity (in two dimensions)

$$\frac{1}{PQ} = \mathrm{div}_Q\,\frac{\boldsymbol{PQ}}{PQ},$$

we obtain

$$I_{0000} = \iint_S \mathrm{d}S_P\,\left\{\int_C \frac{\boldsymbol{PQ}}{PQ}\cdot\boldsymbol{n}_Q\,\mathrm{d}l_Q\right\} = -\int_C \boldsymbol{n}_Q\,\mathrm{d}l_Q\cdot\iint_S \frac{\boldsymbol{QP}}{QP}\,\mathrm{d}S_P$$

where C is the perimeter and $\boldsymbol{n}_Q$ the outer normal vector in Q.

Making use now of

$$\frac{\boldsymbol{QP}}{QP} = \nabla_P\,QP,$$

we obtain

$$I_{0000} = -\int_C \boldsymbol{n}_Q\,\mathrm{d}l_Q\cdot\int_C QP\,\boldsymbol{n}_P\,\mathrm{d}l_P = -\int_C\int_C PQ\,\boldsymbol{n}_P\cdot\boldsymbol{n}_Q\,\mathrm{d}l_P\,\mathrm{d}l_Q.$$

Finally, for a rectangular shape

$$I_{0000} = -2\int_0^l\int_0^l \left(|x-x'| - \sqrt{(x-x')^2+b^2}\right)\mathrm{d}x\,\mathrm{d}x'$$

$$-2\int_0^b\int_0^b (|y-y'| - \sqrt{(y-y')^2+l^2})\,\mathrm{d}y\,\mathrm{d}y',$$

which gives

$$I_{0000} = 2\,b^2\,l\,\sinh^{-1}\left(\frac{l}{b}\right) + 2\,b\,l^2\,\sinh^{-1}\left(\frac{b}{l}\right) + \tfrac{2}{3}\,(b^3+l^3) - \tfrac{2}{3}\,(b^2+l^2)^{3/2}.$$

A.2.2. *Other cases*

Making use of the identity

$$\frac{1}{\sqrt{(x-x')^2+(y-y')^2}} = \lim_{\epsilon\to 0}\frac{1}{\pi}\,\mathrm{Re}\left\{\int_{-\pi/2}^{\pi/2}\mathrm{d}\theta\int_0^\infty \mathrm{d}k\,\mathrm{e}^{-k\,\epsilon}\,\mathrm{e}^{\mathrm{i}k\,[(x-x')\cos\theta+(y-y')\sin\theta]}\right\},$$

https://doi.org/10.1017/S0022112000002871 Published online by Cambridge University Press

one obtains the sextuple integral

$$I_{mnpq} = \lim_{\epsilon\to 0} \frac{1}{\pi} \operatorname{Re}\left\{ \int_{-\pi/2}^{\pi/2} \mathrm{d}\theta \int_0^\infty \mathrm{d}k\, \mathrm{e}^{-k\epsilon} \int_0^l \mathrm{d}x \int_0^l \mathrm{d}x' \right.$$

$$\left. \times \int_0^b \mathrm{d}y \int_0^b \mathrm{d}y' \cos\lambda_m x \cos\lambda_n x' \cos\mu_p y \cos\mu_q y' \, \mathrm{e}^{\mathrm{i}k[(x-x')\cos\theta+(y-y')\sin\theta]} \right\}.$$

The integrations in x, x', y, y' are performed easily, by setting $x = u\,l/\pi$, $x' = u'\,l/\pi$, $y = v\,b/\pi$, $y' = v'\,b/\pi$. We obtain

$$\int_0^\pi \cos m u \, \mathrm{e}^{\mathrm{i}(kl/\pi)u\cos\theta}\,\mathrm{d}u = \mathrm{i}\,\frac{\pi k\, l\, \cos\theta}{\pi^2 m^2 - k^2 l^2 \cos^2\theta}\,[(-1)^m \mathrm{e}^{\mathrm{i}kl\cos\theta} - 1]$$

and similar expressions for the u', v and v' integrations. One obtains finally

$$I_{mnpq} = \frac{8\,b^4\,l^4}{\pi} \int_0^{\pi/2} \mathrm{d}\theta \int_0^\infty \mathrm{d}k\, k^4 \cos^2\theta \sin^2\theta$$

$$\times \frac{1-(-1)^m \cos(kl\cos\theta)}{(\pi^2 m^2 - k^2 l^2 \cos^2\theta)(\pi^2 n^2 - k^2 l^2 \cos^2\theta)}$$

$$\times \frac{1-(-1)^p \cos(kb\sin\theta)}{(\pi^2 p^2 - k^2 b^2 \sin^2\theta)(\pi^2 q^2 - k^2 b^2 \sin^2\theta)}$$

when $m+n$ and $p+q$ are both even. I_{mnpq} is zero in the other cases.

The double integration can easily be carried out numerically. One may also perform the k integral via the residue theorem, the drawback being that many different cases must be distinguished, depending on whether m and n on one side, p and q on the other, are zero or equal or different. So the residue theorem was applied only in the cases $m \neq n$, $p \neq q$, $m,n,p,q \neq 0$, and $m = n \neq 0$, $p = q = 0$, the latter yielding the J_{n0} functions. It is described below. In the other cases I_{mnpq} is calculated via the double integration.

A.2.3. *Calculation of I_{mm00} via the residue theorem*

We further assume m to be odd (the same final result is obtained with m even). The double integral to evaluate is

$$I_{mm00} = \frac{8}{\pi}\,l^4 \int_0^{\pi/2} \frac{\cos^2\theta}{\sin^2\theta}\,\mathrm{d}\theta \int_0^\infty \frac{[1-\cos(kb\sin\theta)]\,[1+\cos(k\,l\,\cos\theta)]}{(m^2\pi^2 - k^2 l^2\cos^2\theta)^2}\,\mathrm{d}k$$

or, setting $k\,l\cos\theta = x$ and $r = b/l$:

$$I_{mm00} = \frac{8}{\pi}\,l^3 \int_0^{\pi/2} \frac{\cos\theta}{\sin^2\theta}\,\mathrm{d}\theta \int_0^\infty \frac{[1-\cos(x\,r\,\tan\theta)]\,[1+\cos x]}{(m^2\pi^2 - x^2)^2}\,\mathrm{d}x.$$

Take

$$I = \int_0^\infty \frac{[1-\cos(x\,r\,\tan\theta)]\,(1+\cos x)}{(m^2\pi^2 - x^2)^2}\,\mathrm{d}x.$$

It can be written

$$I = \frac{1}{2}\operatorname{Re}\left\{ \int_{-\infty}^\infty \frac{1 + \mathrm{e}^{\mathrm{i}x} - \mathrm{e}^{\mathrm{i}r\tan\theta\,x} - \frac{1}{2}\mathrm{e}^{\mathrm{i}(r\tan\theta+1)x} - \frac{1}{2}\mathrm{e}^{\mathrm{i}|r\tan\theta-1|x}}{(m^2\pi^2 - x^2)^2}\,\mathrm{d}x \right\}.$$

https://doi.org/10.1017/S0022112000002871 Published online by Cambridge University Press

The contribution of a remote semi-circular contour in the upper half-plane is zero. Hence I is equal to $\mathrm{i}\pi$, the sum of the two residues in $\pm m\,\pi$. We obtain

$$\int_0^\infty \frac{[1-\cos(x\,r\,\tan\theta)]\,[1+\cos x]}{(m^2\,\pi^2-x^2)^2}\,\mathrm{d}x = \frac{1}{4\,m^2\,\pi}\,f(r,m,\theta)$$

where

$$f(r,m,\theta)=1 \quad \text{for } r\,\tan\theta>1,$$
$$f(r,m,\theta)=1+(r\,\tan\theta-1)\cos(m\,\pi\,r\,\tan\theta)-\frac{\sin(m\,\pi\,r\,\tan\theta)}{m\,\pi} \quad \text{for } r\,\tan\theta<1.$$

To perform the θ integration we introduce θ_0 such that $\theta_0=\arctan(l/b)$. I_{mm00} is finally obtained as

$$I_{mm00}=\frac{2\,l^3}{m^2\,\pi^2}\left\{\int_0^{\theta_0}\frac{\cos\theta}{\sin^2\theta}\left[1+(r\,\tan\theta-1)\cos(m\,\pi\,r\tan\theta)-\frac{\sin(m\,\pi\,r\tan\theta)}{m\,\pi}\right]\mathrm{d}\theta\right.$$
$$\left.+\int_{\theta_0}^{\pi/2}\frac{\mathrm{d}(\sin\theta)}{\sin^2\theta}\right\}.$$

That is, setting $r\tan\theta=u$

$$I_{mm00}=\frac{2\,l^3}{m^2\,\pi^2}\left\{\int_0^1\frac{r^2}{u^2\sqrt{u^2+r^2}}\left[1+(u-1)\cos(m\,\pi\,u)-\frac{\sin(m\,\pi\,u)}{m\,\pi}\right]\mathrm{d}u+\frac{1}{\sin\theta_0}-1\right\}.$$

A.3. *Ice channel*

The integral

$$\tilde{I}_{mn}=\int_{-\infty}^{\infty}\mathrm{d}u\int_0^b\mathrm{d}y\int_0^b\mathrm{d}y'\,\mathrm{e}^{\mathrm{i}k_0\,u}\frac{\cos\mu_m y\,\cos\mu_n y'}{\sqrt{u^2+(y-y')^2}}$$

needs to be evaluated, where m and n are both even.

Setting $u=bU$, $y=bY$, $y'=bY'$, we obtain:

$$\tilde{I}_{mn}=b^2\int_{\infty}^{\infty}\mathrm{d}U\int_0^1\mathrm{d}Y\int_0^1\mathrm{d}Y'\,\mathrm{e}^{\mathrm{i}k_0\,b\,U}\,\frac{\cos m\pi\,Y\,\cos n\pi\,Y'}{\sqrt{U^2+(Y-Y')^2}}.$$

First the U integral is considered. It is transformed via integration in the upper half of the complex plane, with a cut from the branch point $z=\mathrm{i}\,|Y-Y'|$ up the imaginary axis. We obtain

$$\tilde{I}_{mn}=2\,b^2\int_0^1\mathrm{d}Y\int_0^1\mathrm{d}Y'\int_{|Y-Y'|}^{\infty}\mathrm{d}V\,\mathrm{e}^{-k_0\,b\,V}\,\frac{\cos m\pi\,Y\,\cos n\pi\,Y'}{\sqrt{V^2-(Y-Y')^2}}$$

or, setting $V=|Y-Y'|\cosh\psi$:

$$\tilde{I}_{mn}=2\,b^2\int_0^{\infty}\mathrm{d}\psi\int_0^1\mathrm{d}Y\int_0^1\mathrm{d}Y'\,\mathrm{e}^{-k_0\,b\,|Y-Y'|\cosh\psi}\cos m\pi\,Y\,\cos n\pi\,Y'.$$

https://doi.org/10.1017/S0022112000002871 Published online by Cambridge University Press

The Y and Y' integrations are now performed. We obtain, after some algebra

$$\int_0^1 \mathrm{d}Y \int_0^1 \mathrm{d}Y'\, \mathrm{e}^{-\alpha|Y-Y'|} \cos m\pi Y \cos n\pi Y' = \frac{\alpha\,\delta_{mn}(1+\delta_{m0})}{m^2\pi^2+\alpha^2} - 2\frac{\alpha^2\ (1-\mathrm{e}^{-\alpha})}{(m^2\pi^2+\alpha^2)\,(n^2\pi^2+\alpha^2)}$$

(m and n being both even).

Putting back $\alpha = k_0 b \cosh\psi$, the ψ integration of the first term in the above expression is straightforward. Taking finally $u = \tanh\psi$ as the integration variable, we obtain

$$\tilde{I}_{mn} = \frac{b^2\pi\,\delta_{mn}\,(1+\delta_{m0})}{\sqrt{k_0^2 b^2 + m^2\pi^2}} - 4k_0^2 b^4 \times \int_0^1 \frac{1-\mathrm{e}^{-k_0 b/\sqrt{1-u^2}}}{(k_0^2 b^2 + m^2\pi^2 - m^2\pi^2 u^2)\,(k_0^2 b^2 + n^2\pi^2 - n^2\pi^2 u^2)}\,\mathrm{d}u.$$

REFERENCES

Fox, D. W. & Kuttler, J. R. 1983 Sloshing frequencies. *Z. Angew Math. Phys.* **34**, 668–696.

Henrici, P., Troesch, B. A. & Wuytack, L. 1970 Sloshing frequencies for a half-space with circular or strip-like aperture. *Z. Angew Math. Phys.* **21**, 285–317.

Marchenko, A. V. 1997 Resonance interactions of waves in an ice channel. *J. Appl. Maths Mech.* **61**, No. 6, 931–940.

Miles, J. W. 1972 On the eigenvalue problem for fluid sloshing in a half space. *Z. Angew Math. Phys.* **23**, 861–869.

Newman, J. N. 1977 *Marine Hydrodynamics*. MIT Press.

Troesch, B. A. 1973 Sloshing frequencies in a half-space by Kelvin inversion. *Pacific J. Math.* **47**, No. 2, 539–552.

Troesch, B. A. & Troesch, H. R. 1972 A remark on the sloshing frequencies in a half-space. *Z. Angew Math. Phys.* **23**, 703–711.

https://doi.org/10.1017/S0022112000002871 Published online by Cambridge University Press